

Article

Signal Classification of Submerged Aquatic Vegetation Based on the Hemispherical–Conical Reflectance Factor Spectrum Shape in the Yellow and Red Regions

Fernanda Sayuri Yoshino Watanabe ^{1,*}, Nilton Nobuhiro Imai ², Enner Herenio Alcântara ², Luiz Henrique da Silva Rotta ¹ and Alex Garcez Utsumi ¹

¹ Graduate Program in Cartographic Sciences, College of Science and Technology, Sao Paulo State University (UNESP), Rua Roberto Simonsen, 305, Presidente Prudente, SP 19060, Brazil;

E-Mails: luizhrotta@yahoo.com.br (L.H.S.R.); alex_utsumi@yahoo.com.br (A.G.U)

² Department of Cartography, College of Science and Technology, Sao Paulo State University (UNESP), Rua Roberto Simonsen, 305, Centro Educacional, Presidente Prudente, SP 19060, Brazil;

E-Mails: nnimai@fct.unesp.br (N.N.I.); enner@fct.unesp.br (E.H.A.)

* Author to whom correspondence should be addressed; E-Mail: fernandasyw@gmail.com; Tel.: +55-18-3229-5414.

Received: 20 February 2013; in revised form: 25 March 2013 / Accepted: 25 March 2013 /

Published: 15 April 2013

Abstract: The water column overlying the submerged aquatic vegetation (SAV) canopy presents difficulties when using remote sensing images for mapping such vegetation. Inherent and apparent water optical properties and its optically active components, which are commonly present in natural waters, in addition to the water column height over the canopy, and plant characteristics are some of the factors that affect the signal from SAV mainly due to its strong energy absorption in the near-infrared. By considering these interferences, a hypothesis was developed that the vegetation signal is better conserved and less absorbed by the water column in certain intervals of the visible region of the spectrum; as a consequence, it is possible to distinguish the SAV signal. To distinguish the signal from SAV, two types of classification approaches were selected. Both of these methods consider the hemispherical–conical reflectance factor (HCRF) spectrum shape, although one type was supervised and the other one was not. The first method adopts cluster analysis and uses the parameters of the band (absorption, asymmetry, height and width) obtained by continuum removal as the input of the classification. The spectral angle mapper (SAM) was adopted as the supervised classification approach. Both approaches tested different wavelength intervals in the visible and near-infrared spectra. It was demonstrated that the

585 to 685-nm interval, corresponding to the green, yellow and red wavelength bands, offered the best results in both classification approaches. However, SAM classification showed better results relative to cluster analysis and correctly separated all spectral curves with or without SAV. Based on this research, it can be concluded that it is possible to discriminate areas with and without SAV using remote sensing.

Keywords: hyperspectral; submerged aquatic vegetation; cluster analysis; spectral angle mapper; continuum removal

1. Introduction

Submerged aquatic vegetation (SAV) is an important component of aquatic ecosystems and contributes to an increase in habitat diversity by participating in the nutrient cycle as the base of the food chain [1,2]. SAV also serves as a refuge or nursery for plant and animal communities and helps prevent coastline erosion [3]. Despite this important role, SAV can develop dense and widespread colonies in areas where the ecological balance has already been broken [4]. For hydroelectric reservoirs, the occurrence of aquatic plants can be problematic for energy production by decreasing the efficiency [5] due to the clogging of turbine gates and water flow stoppage. This fact leads to an increased interest in monitoring the SAV footprint in reservoirs.

The main factors that contribute to the area of colonization by SAV are the electric conductivity, fetch, vertical attenuation coefficient (light availability within the water column) [6,7], distance from the main water body of the reservoir, and morphometric variables (e.g., the area, coastline slope, and depth) [6]. The temperature also affects the development of such aquatic plants by directly influencing the plant germination [8].

The traditional way to map and discriminate species of SAV requires intensive field work, collateral, ancillary and taxonomical data analysis [9]. On the other hand, remote sensing techniques can offer an economical and fast way to discriminate and estimate biophysical–chemical properties of SAV species. Furthermore, remote sensing can cover broad areas, and its repeated overpass allows the creation of a database for detection of changes over time. Another advantage is the integration in a Geographic Information System (GIS), allowing for a more elaborate analysis [10].

Remote sensing images are used to map SAV colonization; however, this approach presents difficulties and limitations [11–15] similar to those encountered in the identification of other submerged targets, such as coral reefs, substrate types and benthic communities [16–19].

SAV spectral detection is affected by optically active water components (OACs) present in natural water that modifies the apparent and inherent optical properties responsible for light attenuation in the water body [15,20,21]. OACs, such as chlorophyll and suspended solids, may have similar spectral characteristics [22–25] and mask the SAV signal [26–29], respectively. Other factors that can affect the spectral detection of these plants include the weather conditions, sunlight, the angle of view that determines the bidirectional reflectance distribution function [15], water column depth, and the bottom cover type [12].

One of the first works concerning SAV mapping using remote sensing data was published by [11]. The authors compared the multispectral images classification of the MSS (Multispectral Scanner

System) and TM (Thematic Mapper) sensors to detect SAV. It was verified that the water column over the canopy caused errors in classification. Other approaches, such as discriminate analysis and different band ratios (water, vegetation and accessory pigments), using images of NOAA/AVHRR (National Oceanic and Atmospheric Administration/ Advanced Very High Resolution Radiometer) have also been published [12]. There are studies that have adopted images of airborne sensors, such as Daedalus [13] and HyMap [15,30].

Techniques like spectral mixture analysis (SMA), spectral angle mapping (SAM), or the decision tree were used in distinction procedure of submerged and emerged aquatic vegetation [30]. Images of high spatial resolution, such as QuickBird and empirical modeling, are used for mapping SAV [31,32]. Among the approaches currently used, the inversion of semi-analytical models and hyperspectral imaging, commonly seen in studies in ocean waters, stand out the most. These models allow the simultaneous retrieval of the water quality optical parameters concentrations [33,34], the bathymetry [17,35,36], and the substrate composition of the aquatic environment [2].

However, analytical and semi-analytical models require bio-optical measurements (specific inherent optical properties) whose costs of equipment and laboratory tests are still expensive. Recent studies using techniques such as Maximum Likelihood and SAM to classify hyperspectral images (*i.e.*, Airborne Hyperspectral Scanner (AHS)) in order to map seagrass, obtained good results [37].

The majority of submerged aquatic plant mapping studies based on remote sensing images have adopted the same spectral bands that are commonly chosen to classify land vegetation [11,14,15,38], such as the red edge, which indicates the presence of chlorophyll in the leaves, through the absorption by chlorophyll in the red spectral region [39–42], and the near-infrared [43,44]. However, these spectral bands may not be effectively used for plants that grow underwater because the water overlying the vegetation canopies reduces the vegetation effects of red absorption and the near-infrared HCRF.

On the other hand, the penetration of the radiation is greater in the region of the visible spectrum and for this reason it is assumed that this region is more suitable for the identification of SAV [45]. The spectral HCRF of water without SAV has a larger HCRF at 560 nm than the spectral HCRF of SAV found near the surface [14,46]. This wavelength is also strongly correlated to the spectral response of algae chlorophyll [25].

The hypothesis tested in this work is whether it is possible to classify (discriminate) the SAV remote sensing signal using the visible spectral region using information about the shape of the HCRF spectra when the height of the water column over the plant canopy could be considered optically shallow waters.

The objectives of this study were to distinguish the HCRF spectra derived from SAV from bottom without SAV and evaluate different hyperspectral classification approaches using the shapes information of the HCRF spectral curves.

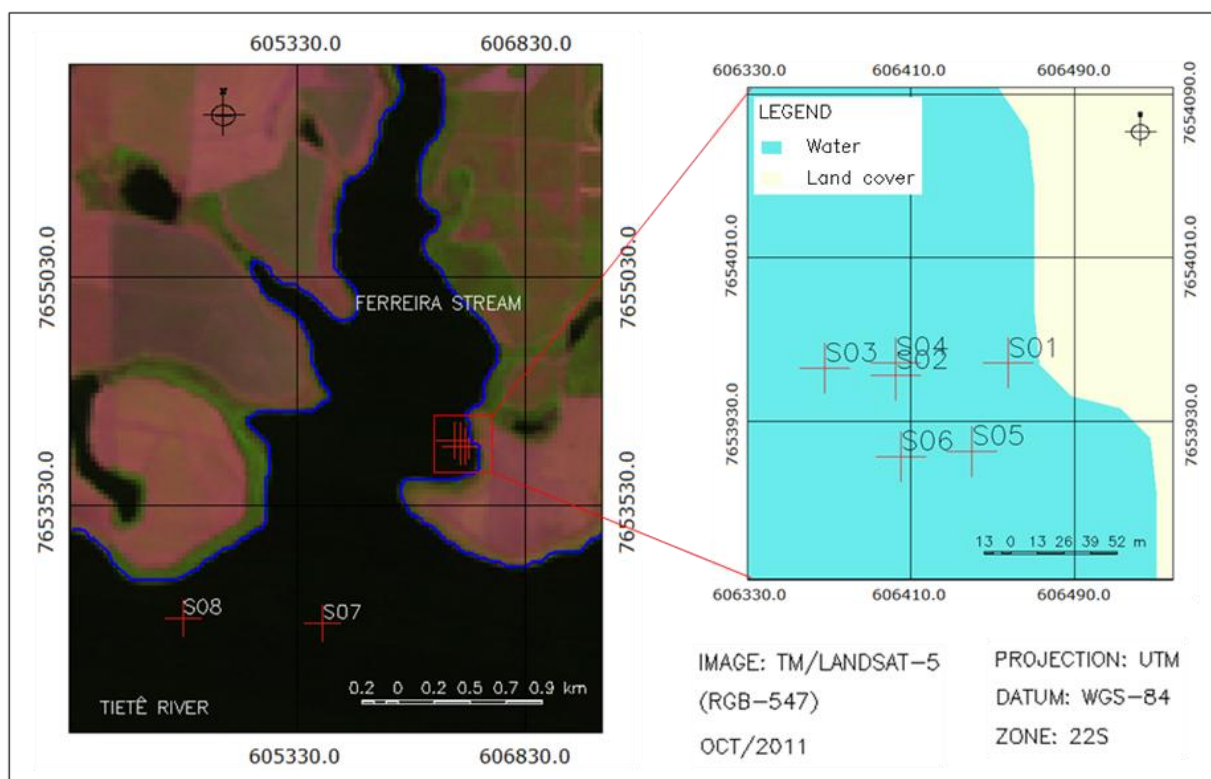
2. Materials and Methods

2.1. Study Area

The study was performed using sample data collected from the Ferreira stream, one of the tributaries of the Tietê River in São Paulo State, which is part of the Nova Avanhandava Reservoir.

Figure 1 shows the region where the data were collected based on TM/Landsat-5 multispectral sensor images in October 2011. The red marks on the illustration represent the sites where the radiometric data were collected. The classified image to the right shows the position of the collection sites within the Ferreira stream.

Figure 1. Study area—observation sites in the Ferreira stream and Tietê Channel, Nova Avanhandava Reservoir, Tietê River, São Paulo State.



2.2. Field Survey

The field survey was carried out from 27 to 29 September 2011 (spring). The selection of this month is due to the conditions of low rainfall and development of submerged aquatic vegetation. In September, it is possible to find submerged canopies under different heights of the water column, which is an important factor for this study.

At every sampling station, the HCRF data were collected using an ASD FieldSpec® portable spectroradiometer, model HandHeld UV/VNIR and the software RS3, to measure the water leaving radiance of the water at each sampling station during water sampling. The instrument records a continuous spectrum in 512 bands, ranging from 274 nm to 1,085 nm with 1,587 nm spectral resolution [47]. At each sampling station, the reference panel (white Spectralon panel) was scanned first.

The water leaving radiance was measured keeping the sun-sensor azimuth at 90° and aiming at the water surface at a 45° zenith angle to reduce sky radiance and the surface reflectance [21]. Each of the sampled spectra was the average of ten readings (sample size), which were afterwards averaged to minimize random effects.

From the measurements made, the hemispherical-conical reflectance factor—HCRF (dimensionless) was estimated by the ratio of the radiance of the target (water leaving radiance), L ($W\ m^{-2}\ sr^{-1}$), and

the panel Spectralon radiance, L_p ($\text{W m}^{-2} \text{sr}^{-1}$), for each recorded measurement multiplied by calibration factor of the white reference panel, Cal (dimensionless), provided by manufacturer, for each wavelength (λ) as shown in Equation (1).

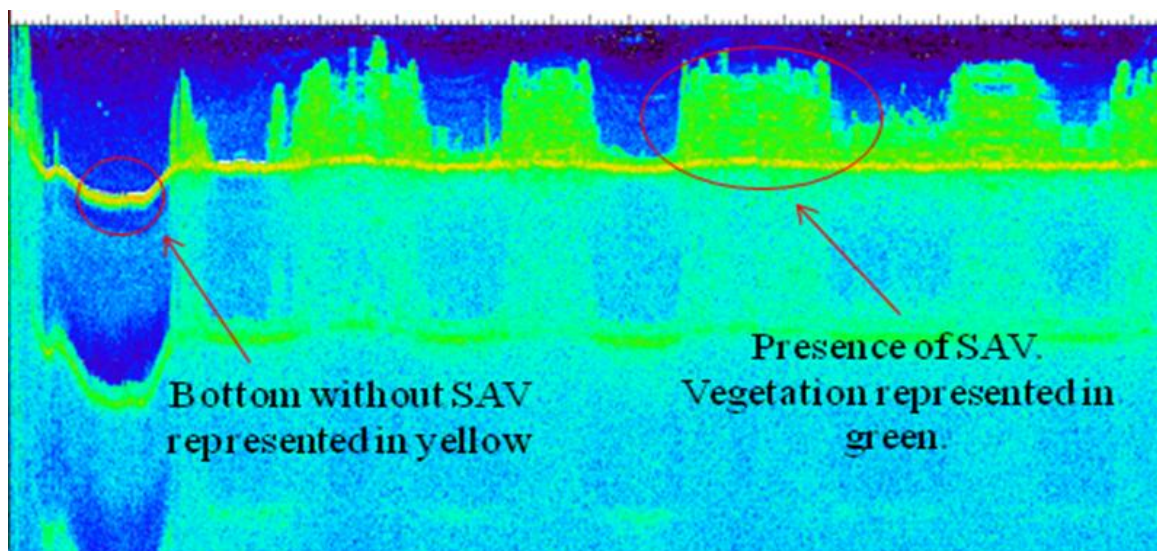
$$HCRF = \frac{L(\lambda)}{L_p(\lambda)} \times Cal(\lambda) \quad (1)$$

At the same sampling locations and at the same time of measurements of HCRF, turbidity (NTU, determined by a portable digital/bench turbidimeter, model AP 2000) was collected [48]. This data was collected to give a basic characterization of the water transparency.

Hydroacoustic data were collected to support the survey using a DT-X Portable Echosounder that works in dual frequency [49]. This echo sounder collects data using the software Visual Acquisition, allowing for the determination of the depth, height and cover density of SAV [50]. SAV height data were used to select the survey sites. These data were helpful when identifying colonized and non-colonized areas for plants in cases where it was not possible to visually detect the plants.

During the hydroacoustic data collection, the software Visual Acquisition generates an ecograma, where it is possible to view the presence or absence of SAV, thereby defining the sampling stations. The ecograma generated at the instant of taking of the data is similar to what can be viewed after collection in the software Visual Analyzer (Figure 2).

Figure 2. Ecograma generated by software Visual Analyzer similar to that produced instantly during the taking of data.



As shown in Figure 1, data were collected from eight different sites. Due to different characteristics at each site, more than one sample from different locations was collected, and a total of 20 HCRF samples were measured (see Table 1 for a detailed account of samples in each site). Sites both with and without SAV were selected. For those sites with SAV, areas with different water column depths over the canopy were chosen. Note that two sites were located in the Tietê river channel because the Ferreira stream did not contain environments without SAV and were deeper than 10 m.

Table 1 shows certain characteristics of the data sampling locations, such as the channel, name of the site, name of the sample, the presence of SAV, the water column height over the SAV and the turbidity.

Table 1. Location and turbidity of the collection sites as well as the presence of SAV and the water column height over the SAV canopy.

Sites	Turbidity (NTU)	Channel	Samples	SAV	Water Column Height over the SAV (m)
S01	1.98	Ferreira stream	1	NO	-
			2	YES	0.15
			3	YES	0.01
S02	1.31	Ferreira stream	4	YES	0.2
			5	YES	2.0
			6	YES	0.46
			7	YES	0.07
			8	NO	-
S03	2.16	Ferreira stream	9	NO	-
			10	YES	3.0
			11	YES	0.63
S04	1.67	Ferreira stream	12	YES	1.0
			13	YES	0.22
			14	YES	0.15
S05	1.41	Ferreira stream	15	YES	0.3
			16	YES	0.5
			17	YES	0.05
S06	1.45	Ferreira stream	18	YES	2.0
S07	1.2	Tietê River	19	NO	-
S08	1.2	Tietê River	20	NO	-

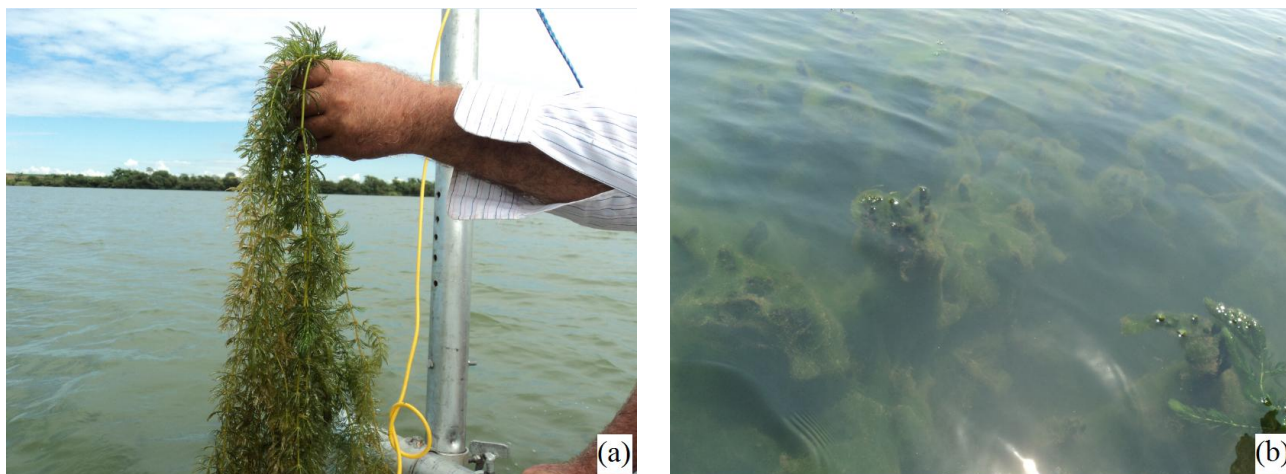
The majority of the samples were collected in areas with SAV and ranged from 0.01 to 3 m in water column height over the SAV. Samples without SAV were also well represented: shallow coastline with 1 m depth (S01), areas with 6 m depth where the presence of SAV is possible (S03) and deeper sites with depths of 15 and 20 m (S07 and S08).

The turbidity was low at all sites with a range of 1.2 to 2.16 NTU; the low turbidity level was mainly related to low rainfall during the data collection period. This low turbidity was beneficial to this study because it reduced the influence of inherent optical properties that can mask the spectral response of the SAV signal recorded by the sensor. Lower turbidity levels were observed at sites located in the channel of the Tietê River, whereas small channels, such as the Ferreira stream, are more influenced by the input of sediments from adjacent areas than large channels.

Despite the good weather conditions (*i.e.*, low clouds that do not hampered the radiometric data collection and rainfall) and low turbidity observed in September in this region, the HCRF data collection was hampered by ripples formed by the wind on the surface of the water.

The largest development of SAV in the Nova Avanhandava Reservoir, verified by [5], is related to the spatial location of the reservoir near the end of the Tietê River reservoirs chain system, causing favorable conditions for the concentration of nutrients and the development of a clear water column. *Ceratophyllum demersum* was predominant during the data collection period (see Figure 3).

Figure 3. Study area infested by *Ceratophyllum demersum*. (a) SAV removed from a boat motor. (b) Infestation by *Ceratophyllum demersum* and periphyton.



2.3. Data Analysis

The HCRF data collected during the field campaign were analyzed using methods such as cluster analysis [51], continuum-removal technique [52] and the spectral angle mapper (SAM) [53].

2.3.1. Continuum-Removal Technique

Continuum removal is a technique intended to isolate and analyze a specific absorption feature of a spectrum [54]. This technique is commonly used to analyze mineral absorption features [52,54], to map different types of vegetation and assess their health condition [55–57], and to analyze water body data [58].

Straight line segments are connected to the absorption band limits (maximum reflectance points) such that the continuum of each absorption feature is determined [52,58]. The equation of this line is used as a reference to calculate the angle between this line and the original curve:

$$\rho_{Continuum\lambda} = k\lambda + w \quad (2)$$

where $\rho_{Continuum\lambda}$ is the spectrum continuum for the same wavelength of $\rho_{Original\lambda}$ (beam), which is the value of the original spectrum; λ is the wavelength; k is the angle coefficient; and w is the linear coefficient. The ratio between $\rho_{Original\lambda}$ and $\rho_{Continuum\lambda}$ is called the continuum removal factor ($\rho_{CR\lambda}$):

$$\rho_{CR\lambda} = \frac{\rho_{Original\lambda}}{\rho_{Continuum\lambda}} \quad (3)$$

Based on the removed continuum, it is possible to obtain measurements that determine absorption features such as the wavelength depth, feature absorption area, wavelength range width and asymmetry [33]. These features are associated with the shape of the absorption wavelength range and were used as input data for the classification by cluster analysis.

2.3.2. Cluster Analysis

From the HCRF spectral data, it is possible to identify spectral signatures according to the water column characteristics. One approach to identifying such curves is the use of clustering of data related to reflectance by defining the spectral classes. The first classification approach used in this study was

hierarchical clustering analysis [59]. In this paper, the features of an absorption wavelength range obtained with continuum removal were used as variables in cluster analysis.

Hierarchical clustering analysis uses similarity measurements obtained by calculating distances that indicate the proximity between clusters [59]. Important factors should be considered when selecting a distance measurement approach such as nature of the variables (discrete, continuous) and scales of measurements (ordinary, interval, ratio) [51]. In this context, the distance between clusters was defined via a linkage method [42].

Minitab [60] statistic software was adopted to apply the cluster analysis for the observed data. The data were standardized to minimize the effect of differences in the magnitude between the variables (band parameters). Different linkage and similarity measurements were evaluated in order to determine a suitable approach, and the average linkage method and Euclidean distance were selected as the appropriate measures. A similarity level of 95 was adopted.

2.3.3. Spectral Angle Mapper (SAM)

The other classification method used was a supervised approach using SAM, an algorithm developed by Joe W. Boardman [61]. This method computes the extent of similarity among the analyzed spectral vector data, test vectors and reference spectral vectors, based on the obtained angle between these vectors, where the vectors are considered to have a dimension equal to the number of bands (*nb*) [53]. This method has been applied for several purposes, such as mineral prospect mapping [62], land cover mapping [63,64], vegetation mapping [65] and water body HCRF spectrum analysis [58,66] including water macrophyte mapping [15].

The following equation presents the calculation of the spectral angle between a test vector (*t*) and a reference vector (*r*):

$$\cos^{-1} \left(\frac{\vec{t} \cdot \vec{r}}{\|\vec{t}\| \|\vec{r}\|} \right) \tag{4}$$

This equation is also represented as

$$\cos^{-1} \left(\frac{\sum_{i=1}^{nb} t_i r_i}{\left(\sum_{i=1}^{nb} t_i^2 \right)^{\frac{1}{2}} \left(\sum_{i=1}^{nb} r_i^2 \right)^{\frac{1}{2}}} \right) \tag{5}$$

This similarity measure is independent of the gain factors because the angle between two vectors does not vary relative to the vector magnitude [52]. SAM method considers only the curve shape and is not affected by differences in the width among the spectra [66].

The SAM algorithm was written and implemented in MATLAB [67] software to classify the spectral data. Eight of the original 20 HCRF curves were selected as reference vectors. These reference vectors represent different environmental conditions observed in the study case. The selection of these vectors was based on the water depth and the water column height over the SAV.

3. Results and Discussion

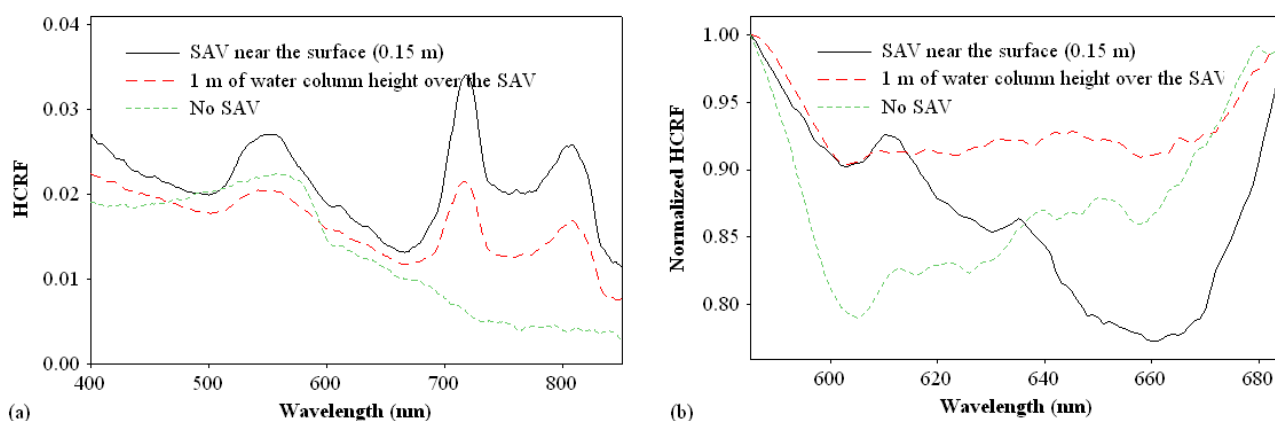
3.1. Continuum Removal

Based on preliminary analyses (exploratory and visual) of the HCRF spectra, variations in the shape and depth of the absorption wavelength range localized in the visible spectrum were observed in the interval corresponding to the green to red edge range (560 to 700 nm), and another from red edge to near-infrared range (700 to 810 nm).

It was observed that the different behavior of these absorption wavelength ranges seemed to be related to variations in environmental collection, as well as the presence and absence of SAV and the water column height over the macrophytes canopy. One method to evaluate the behavior of these absorption wavelength ranges is the continuum-removal technique that allows for the obtaining of the band parameters that were adopted as input data for cluster analysis. The purpose of this process was to consider the shapes of the spectral HCRF curves in this cluster analysis. However, the absence of plants and variations in the water column height cause displacement in the HCRF and absorption peaks, thus hindering the application of one continuum-removal function to all of the spectra.

The spectral interval from 585 to 685 nm yielded the most satisfactory result (*i.e.*, normalized HCRF less than or equal to 1), which adjusted itself to all other HCRF spectra. Figure 4 shows the three normalized HCRF curves obtained by continuum removal of very different environments, thereby allowing for the checking of changes in the behavior of absorption wavelength range in accordance with the presence and absence of SAV and different water column heights over the canopy.

Figure 4. From the results obtained by continuum removal, it is possible to observe differences between curves with and without SAV. **(a)** HCRF spectra of the points 2 (SAV near the surface), 17 (1 m of water column over the canopy), and 20 (no SAV). **(b)** Examples of normalized HCRF spectra obtained by the removed continuum of the 585 to 685 nm interval to three very different environment in terms of presence of SAV and water column height over the SAV canopy.



The normalized HCRF curves shown in Figure 4 represent the different environments present in the data collection area: sites with SAV near the surface, sites with 1 m of water column height over the SAV, and sites without SAV. Differences between the standard curves are readily apparent, most clearly in terms of position and depth of wavelength. For the condition of SAV near the surface, the

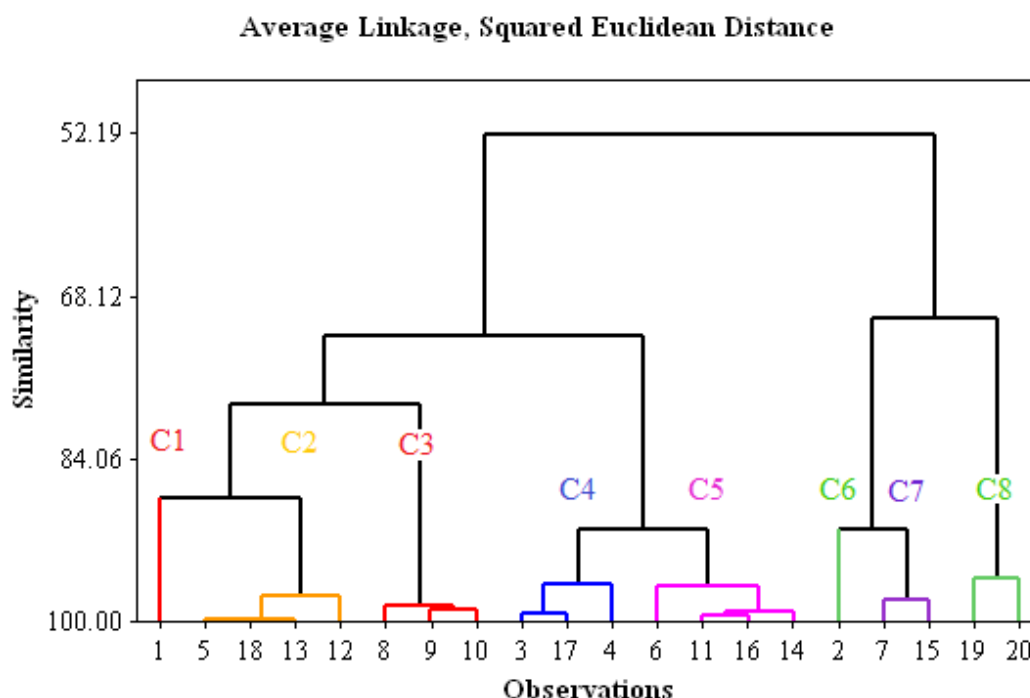
position of the maximum absorption peak appears to be shifted to the left at an approximate wavelength of 660 nm. In contrast, for curves without the presence of SAV, this absorption maximum peak is shifted to the right at approximately 605 nm. For the intermediate cases, where there is a considerable water column height over the SAV, this peak is not well defined.

This shifting can be partially explained through the effect of water column; with the penetration of light in the water its intensity decreases exponentially. This attenuation of light is more severe in the red region than in the blue region of the electromagnetic spectrum. The normalized HCRF for SAV with over 1 m of column water have less of an absorption feature by algal chlorophyll than the near-surface SAV.

3.2. Cluster Analysis Classification

The cluster analysis results using the same interval used in Figure 4, 585 to 685 nm, and presented in a dendrogram, can be accessed in Figure 5. Eight clusters were generated when adopting a similarity of 95. Among these clusters, three are formed by spectra without plants and are separated based on the water column depth at the sampling position.

Figure 5. Cluster analysis: dendrogram based on band parameters for the 585 to 685 nm spectral interval.



Five clusters are formed by spectra with SAV (C2, C4, C5, C6 and C7); however, there is an occasional coincidence with respect to the water column height over SAV of the samples. With the exception of spectra 14 (0.22 m), cluster C2 is formed only by curves collected in locations where the water column height over the canopy was greater than 1 m. Cluster C4 comprises curves with a canopy near the surface (0.01–0.2 m). The samples in cluster C5, with the exception of sample 14 (0.15 m), had water column heights over the SAV from 0.4 to 1 m. Cluster C6 comprises only one HCRF

spectrum (sample 2) with 0.15 m water column height over the canopy. The HCRF curves of cluster C7 also do not present a relation with water column height over the canopy.

Clusters C1, C3 and C8 do not present SAV and were grouped based on the range of column depths. Cluster C1 comprises just one sample collected at a site near the coastline with 1 m depth (sample 1). C3 is a unique cluster that represents a classification error being determined by curves with and without SAV. C3 is formed by all HCRF curves collected at site S03, which include two spectra without SAV and one with a water column height over the canopy of 3 m, yielding an error of 33%. Nevertheless, cluster C8 presents a good result; this group comprised samples 19 and 20, both of which were collected in relatively deep (15–20 m) areas of the Tietê River channel (see Figure 1 for location).

3.3. Spectral Angle Mapper (SAM)

The classification by SAM was applied in the wavelength range 585–685 nm of the HCRF spectra, the same range in which it was applied to the continuum removal for generating input data for classification by cluster analysis. Table 2 shows the results of the spectral angle mapping. The first line presents the eight HCRF curves adopted as a reference, and the first column lists the 12 tests that were classified. The numbers in bold correspond to the smallest angles determined between a test spectrum relative to each reference spectrum.

Table 2. Angles obtained by SAM algorithm between the reference vectors (R) and test vectors (T) that determine the degree similarity between two HCRF curves. The numbers in bold correspond to the highest values of similarity among the pairs of vectors (reference and test) formed, i.e., both vectors belong to the same class.

T\R	1	4	7	9	11	14	18	20
2	0.0428	0.0387	0.0122	0.0583	0.0318	0.031	0.0458	0.0752
3	0.0263	0.0265	0.014	0.0523	0.0176	0.0157	0.0377	0.0756
5	0.0166	0.0433	0.0355	0.0267	0.0168	0.0186	0.0127	0.0531
6	0.023	0.0326	0.0194	0.0427	0.0125	0.0128	0.0282	0.0658
8	0.0399	0.0717	0.0614	0.0071	0.0447	0.0466	0.019	0.0298
10	0.0253	0.0561	0.0492	0.0161	0.0299	0.032	0.0109	0.0432
12	0.0126	0.0383	0.0337	0.0326	0.0118	0.0135	0.0181	0.0598
13	0.0168	0.0303	0.0385	0.0455	0.0167	0.018	0.0333	0.0729
15	0.0281	0.0325	0.0143	0.0489	0.0186	0.0178	0.0349	0.0702
16	0.0131	0.0277	0.0305	0.0438	0.0085	0.0094	0.0297	0.0703
17	0.0284	0.0145	0.0193	0.0601	0.0195	0.0174	0.0453	0.0851
19	0.0785	0.1077	0.0905	0.0431	0.0809	0.0827	0.0557	0.0193

The SAM showed superior results compared to those obtained by cluster analysis, as all samples were classified correctly based on the presence or absence of SAV. In the SAM case, curve 10 (3 m water column height over the SAV) was grouped incorrectly as a sample without SAV by cluster analysis was classified by SAM together with samples with a water column height over the canopy from 1 to 2 m. As in the cluster analysis, this technique also generated three classes for HCRF samples without SAV separated by column depth.

Figure 6 shows the HCRF curves separated according to the SAM classes. The classification result is considered good because the main conditions related to the absence or presence of SAV were consistent.

Samples collected at the same sites or with homogenous vegetation cover were classified together. It is important to note that curve 1 represents a different class because it corresponds to the only HCRF measurement taken from shallow water (approximately 1 m depth) without SAV. Another class comprising 4 and 17 features the presence of SAV near the surface with 0.2 m and 0.05 m of water column height over the canopy, respectively. Two HCRF peaks were observed in these curves associated to an SAV-spectral response at 715 nm (red edge) and 805 nm (infrared). However, at these water column heights over the canopy, the infrared HCRF becomes lower relative to the green spectral region peak.

Figure 6. HCRF curves classified by SAM for the 585–685 nm interval. (a) The first class corresponds to shallow environment (1 m) without SAV; (b) the second class comprises for HCRF curves with water column height over SAV canopy between 0.005 and 0.2 m; (c) the third class is also formed for samples with SAV near the surface (0.01–0.3 m); (d) the fourth class comprises of HCRF spectra collected in locations without SAV and water column depth of 6 m; (e) HCRF curves with water column height over SAV from 0.22 m to 1 m; (f) the sixth class has only one HCRF spectrum with 0.15 m of water column height over the SAV; (g) the seventh class present spectra with SAV and with water column height over SAV from 2 to 3 m; (h) the last class comprises of HCRF spectra without SAV and with water column depth from 15 to 20 m.

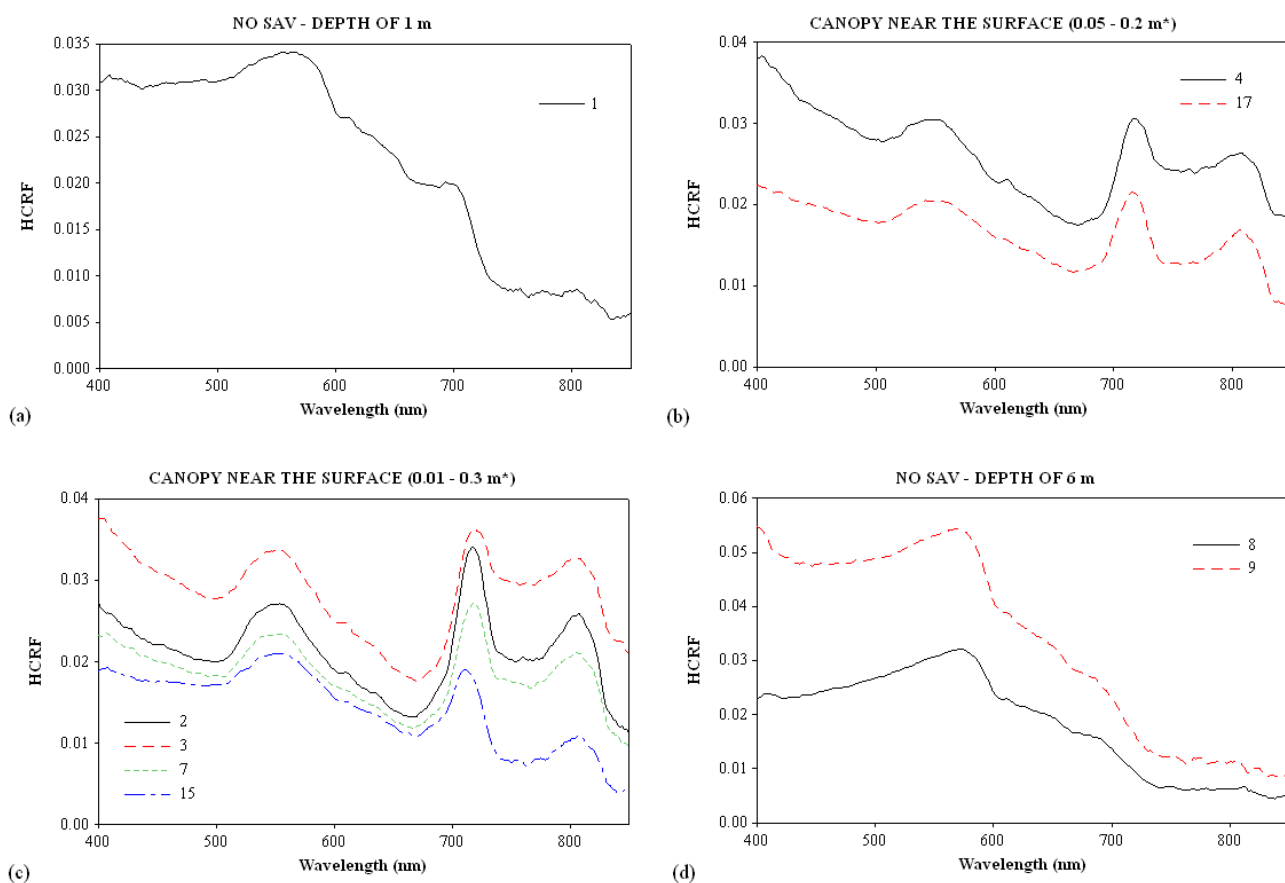
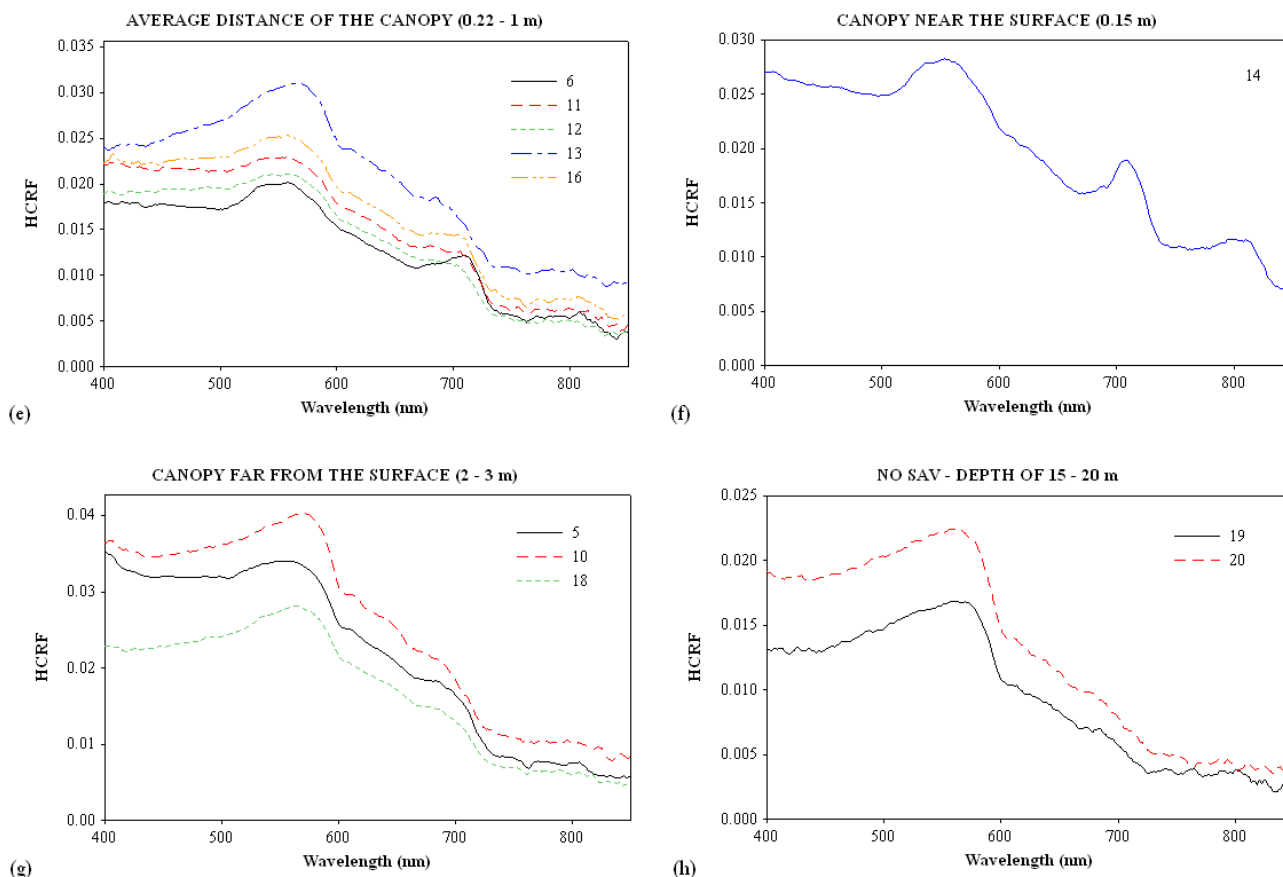


Figure 6. Cont.



Unlike the cluster classification, the SAM classification was able to separate the HCRF curves that were collected from sites without SAV at 6 m depth (samples 8 and 9). These spectral curves do not show any features related to the SAV.

Another class comprises the spectral curves 6, 11, 12, 13 and 16, which also showed a variation in the water column height over the canopy (0.22 m to 1 m). These spectral curves showed a remarkable decrease in the infrared region of the HCRF due to the energy absorption by water.

Another class contains the HCRF curves 2, 3, 7 and 15, which were collected from sites with SAV but with a substantial variation in the water column over the canopy (0.07 m to 0.3 m). These spectra have unique features of the SAV spectral response, such as two infrared peaks and high energy absorption in the red region. All of the other spectral curves, with the exception of curve 15, showed a higher HCRF within the infrared region than within the green region. Spectral curve 3 with a 0.01 m water column also showed a higher HCRF within the infrared region, creating a typical vegetation plateau in that spectral interval. This higher HCRF is due to the relationship between the water column height over the canopy and the energy absorption within the infrared region, which is an indirect effect.

Cluster analysis grouped the HCRF curve 14 with other dissimilar curves (6 (0.46 m), 11 (0.63 m), 14 (0.15 m), 16 (0.5 m)), but the SAM classification did not. Although the water column height above the canopy was the same for the spectra 2 and 14, the spectral curves were different.

Another correct classification result using SAM is the group containing 5, 10 and 18 HCRF curves, which correspond to SAV that could not be observed in the field with 2 to 3 m of water overlying the

canopy. This class was characterized by a low infrared HCRF and the absence of the two HCRF peaks that are generally associated to SAV.

The last identified class comprises the samples 19 and 20, which did not have SAV and had depths of 15 to 20 m. In this case, the water columns can be considered deep, *i.e.*, there is no influence of the bottom signal on these spectral responses. As expected, the spectral curves do not show any features associated with SAV.

In all spectral curves, presented in Figure 6, the high HCRF in the blue region of the spectrum is evident, and this is due to low concentration the chlorophyll algal. High reflectance in the region between 400 and 500 nm are associated with clear water [68], due to the high scattering molecular of the violet and blue light [69]. On the other hand, low reflectance is related with absorption by chlorophyll-*a* [25,68]. Low turbidity in the study area, between 1.2 and 2.16 NTU, shows the low concentration of both algal and non-algal particulate materials.

4. Conclusions

The initial hypothesis that it is possible to classify (discriminate) spectral curves from sites with and without SAV depending on whether the signal is derived from submerged aquatic plants was demonstrated to be true: the visible spectral region offered suitable data of the submerged canopy in optically shallow waters.

From the results of continuum removal, shape patterns of the absorption feature in the range 585–685 nm associated with distance from the canopy SAV or absence of vegetation can be checked. Even a 1 m high column of water on the canopy it was possible to identify the presence of submerged aquatic vegetation only by the asymmetry feature of the absorption band.

This research demonstrates that the both different classification methods that consider the shape of the HCRF spectra yield satisfactory results for SAV identification. In addition, the spectral region that showed the best performance in identifying the SAV was the wavelength interval of 585 to 685 nm, associated with the yellow and red regions.

Cluster analysis showed classifications errors of 33% in cluster C3 and 25% in C5. The error observed in cluster C3 shows that the classifier does not distinguish between the response of the water without plants and SAV under a water column of 3 m. In cluster C5, the point 4 (0.2 m high column of water on the canopy) was collected in a station with 1.98 NTU, slightly larger than points with 0.46 m and 0.5 m (1.31 and 1.41 NTU, respectively).

The elevation of turbidity causes an increase in the attenuation of the radiation in the water column, reducing the final signal of SAV that leaves the water. Despite point 6 (0.63 m height of the water column on the canopy) having higher turbidity than the other points of C5, the attenuation was not enough for the radiation to be confused with the registered points with the water column of 1 m over canopy.

Although there are considerable classification errors in isolated clusters (C3 and C5), the global accuracy of the cluster analysis was 90%. The results show that the classification by cluster analysis using features of the absorption feature obtained with continuous removal can show good results for mapping SAV, especially under conditions of high development.

On the other hand, the supervised classification method based on SAM provided better results that did the cluster analysis algorithm, with 100% accuracy of the classifier. The SAM-based approach was

able to distinguish the four main characteristics of the analyzed sites: SAV independent of the water column height above the canopy; the absence of SAV in shallow waters up to 1 m depth; and, the absence of SAV waters with a depth of 6 m and greater (up to 15 m). However, both approaches did not discriminate the spectral curves with SAV into classes where the heights of the water column above the canopy were similar.

Acknowledgments

We thank the FEPAF and PPGCC for their financial assistance of the survey field data collection and CNPq for a scholarship.

References

1. Esteves, F.A. *Fundamentos de Limnologia*, 2nd ed.; Interciência: Rio de Janeiro, Brazil, 1998.
2. Wetzel, R.G. *Limnology: Lake and River Ecosystems*, 3rd ed.; Elsevier Academic Press: London, UK, 2001.
3. Dekker, A.G.; Brando, V.E.; Anstee, J.M.; Pinnel, N.; Kutser, T.; Hoogeboom, E.J.; Peters, S.; Pasterkamp, R.; Vos, C.; Olbert, C.; Malthus, T.J.M. Imaging Spectrometry of Water. In *Imaging Spectrometry: Basic Principles and Prospective Applications*; van der Meer, F.D., Jong, S.M., Eds.; Kluwer Academic Publishers: New York, NY, USA, 2002; Chapter 11, pp. 307–359.
4. Pitelli, R.L.C.M.; Toffaneli, C.M.; Vieira, E.A.; Pitelli, R.A.; Velini, E.D. Dynamics of the aquatic macrophyte community in the Santana reservoir in Pirai-RJ. *Weed Sci.* **2008**, *26*, 473–480.
5. Cavenaghi, A.L.; Velini, E.D.; Galo, M.L.B.T.; Carvalho, F.T.; Negrisoni, E.; Trindade, M.L.B.; Simionato, J.L.A. Characterization of water quality and sediment related to the occurrence of aquatic plants in five Tietê watershed reservoirs. *Weed Sci.* **2003**, *21*, 43–52.
6. Thomaz, S.M.; Souza, D.C.; Bini, L.M. Species richness and beta diversity of aquatic macrophytes in a large subtropical reservoir (Itaipu Reservoir, Brazil): The influence of limnology and morphometry. *Hydrobiologia* **2003**, *505*, 119–128.
7. Bini, L.M.; Thomaz, S.M. Prediction of *Egeria najas* and *Egeria densa* occurrence in a large subtropical reservoir (Itaipu Reservoir, Brazil-Paraguay). *Aquat. Bot.* **2005**, *83*, 227–238.
8. Rybicki, N.B.; Carter, V. Light and temperature effects on the growth of wild celery and hydrilla. *J. Aquat. Plant Manage.* **2002**, *40*, 92–99.
9. Lee, K.H.; Lunetta, R.S. Wetland Detection Methods. In *Wetland and Environment Applications of GIS*; Lyon, J.G., McCarthy, J., Eds.; Lewis Publishers: New York, NY, USA, 1996; pp. 246–284.
10. Adam, E.; Mutanga, O.; Rugege, D. Multispectral and hyperspectral remote sensing for identification and mapping of wetland vegetation: A review. *Wetlands Ecol. Manag.* **2010**, *18*, 281–296.
11. Ackleson, S.G.; Klemas, V. Remote sensing of submerged aquatic vegetation in lower Chesapeake Bay: A comparison of Landsat MSS to TM imagery. *Remote Sens. Environ.* **1987**, *22*, 235–248.
12. Peñuelas, J.; Gamon, J.A.; Griffin, K.L.; Field, C.B. Assessing community type, plant biomass, pigment composition, and photosynthetic efficiency of aquatic vegetation from spectral reflectance. *Remote Sens. Environ.* **1993**, *46*, 110–118.

13. Malthus, T.J.; George, D.G. Airborne remote sensing of macrophytes in Cefni Reservoir, Anglesey, UK. *Aquat. Bot.* **1997**, *58*, 317–332.
14. Han, L.; Rundquist, D.C. The spectral responses of *Ceratophyllum demersum* at varying depths in an experimental tank. *Int. J. Remote Sens.* **2003**, *24*, 859–864.
15. Hestir, E.L.; Khanna, S.; Andrew, M.E.; Santos, M.J.; Viers, J.H.; Greenberg, J.A.; Rajapakse, S.S.; Ustin, S.L. Identification of invasive vegetation using hyperspectral remote sensing in the California Delta ecosystem. *Remote Sens. Environ.* **2008**, *112*, 4034–4047.
16. Phinn, S.R.; Dekker, A.G.; Brando, V.E.; Roelfsema, C.M. Mapping water quality and substrate cover in optically complex coastal and reef waters: An integrated approach. *Mar. Pollut. Bull.* **2005**, *51*, 459–469.
17. Brando, V.E.; Anstee, J.M.; Wettle, M.; Dekker, A.G.; Phinn, S.R.; Roelfsema, C. A physics based retrieval and quality assessment of bathymetry from suboptimal hyperspectral data. *Remote Sens. Environ.* **2009**, *113*, 755–770.
18. Lyons, M.; Phinn, S.; Roelfsema, C. Integrating Quickbird multi-spectral satellite and field data: Mapping bathymetry, seagrass cover, seagrass species and change in Moreton Bay, Australia in 2004 and 2007. *Remote Sens.* **2011**, *3*, 42–64.
19. Hedley, J.D.; Roelfsema, C.M.; Phinn, S.R.; Mumby, P.J. Environmental and sensor limitations in optical remote sensing of coral reefs: Implications for monitoring and sensor design. *Remote Sens.* **2012**, *4*, 271–302.
20. Kirk, J.T.O. *Light and Photosynthesis in Aquatic Ecosystems*, 2nd ed.; Cambridge University Press: Cambridge, UK, 1994.
21. Mobley, C.D. *Light and Water: Radiative Transfer in Natural Waters*; Academic Press: San Diego, CA, USA, 1994.
22. Gitelson, A. The peak near 700 nm on radiance spectra of algae and water: Relationships of its magnitude and position with chlorophyll concentration. *Int. J. Remote Sens.* **1992**, *13*, 3367–3373.
23. Mittenzwey, K.-H.; Ullrich, S.; Gitelson, A.A.; Kondratiev, K.Y. Determination of chlorophyll *a* of inland waters on the basis of spectral reflectance. *Limnol. Oceanogr.* **1992**, *37*, 147–149.
24. Gitelson, A.; Garbuzov, G.; Szilagyi, F.; Mittenzwey, K.-H.; Karnieli, A.; Kaiser, A. Quantitative remote sensing methods for real-time monitoring of inland waters quality. *Int. J. Remote Sens.* **1993**, *14*, 1269–1295.
25. Rundquist, D.C.; Han, L.H.; Schalles, J.F.; Peake, J.S. Remote measurement of algal chlorophyll in surface waters: The case for the first derivative of reflectance near 690 nm. *Photogramm. Eng. Remote Sensing* **1996**, *62*, 195–200.
26. Goodin, D.G.; Han, L.; Fraser, R.N.; Rundquist, C.; Stebbins, W.A.; Schalles, J.F.; Analysis of suspended solids in water using remotely sensed high resolution derivative spectra. *Photogramm. Eng. Remote Sensing* **1993**, *59*, 505–510.
27. Chen, Z.; Curran, P.J.; Hansom, J.D. Derivative reflectance spectroscopy to estimate suspended sediment concentration. *Remote Sens. Environ.* **1992**, *40*, 67–77.
28. Han, L.; Rundquist, D.C.; Liu, L.L.; Fraser, R.N.; Schalles, J.F. The spectra responses of algal chlorophyll in water with varying levels of suspended sediment. *Int. J. Remote Sens.* **1994**, *15*, 3707–3718.

29. Han, L. Spectral reflectance with varying suspended sediment concentrations in clear and algae-laden waters. *Photogramm. Eng. Remote Sensing* **1997**, *63*, 701–705.
30. Williams, D.J.; Rybicki, N.B.; Lombana, A.V.; O'Brien, T.M.; Gomez, R.B. Preliminary investigation of submerged aquatic vegetation mapping using hyperspectral remote sensing. *Environ. Monit. Assess.* **2003**, *81*, 383–392.
31. Yuan, L.; Zhang, L. Mapping large-scale distribution of submerged aquatic vegetation coverage using remote sensing. *Ecol. Inform.* **2008**, *3*, 245–251.
32. Rotta, L.H.S. Inferência Especial Para Mapeamento de Macrófitas Submersas—Estudo de Caso. M.Sc. Thesis, Universidade Estadual Paulista, Bauru, Brazil, 2011.
33. Clementson, L.A.; Parslow, J.S.; Turnbull, A.R.; McKenzie, D.C.; Rathbone, C.E. Optical properties of waters in Australasian sector of the Southern Ocean. *J. Geophys. Res.* **2001**, *106*, 31611–31625.
34. Brando, V.E.; Dekker, A.G. Satellite hyperspectral remote sensing for estimating estuarine and coastal water quality. *IEEE Trans. Geosci. Remote Sens.* **2003**, *41*, 1378–1387.
35. Lee, Z.; Casey, B.; Arnone, R.; Weidmann, A.; Parsons, R.; Montes, M.J.; Gao, B.C.; Goode, W.; Davis, C.O.; Dye, J. Water and bottom properties of a coastal environment derived from Hyperion data measured from the EO-1 spacecraft platform. *J. Appl. Remote Sens.* **2007**, *1*, 1–16.
36. Lee, Z.L.; Carder, K.L.; Mobley, C.D.; Steward, R.G.; Patch, J.S. Hyperspectral remote sensing for shallow waters: 2. Deriving bottom depths and water properties by optimization. *Appl. Opt.* **1999**, *38*, 3831–3843.
37. Casal, G.; Sánchez-Carnero, N.; Domínguez-Gómez, J.A.; Kutser, T.; Freire, J. Assessment of AHS (Airborne Hyperspectral Scanner) sensor to map macroalgal communities on the Ría de Vigo and Ría de Aldán coast (NW Spain). *Mar. Biol.* **2012**, *159*, 1997–2013.
38. Everitt, J.H.; Yang, C.; Escobar, D.E.; Webster, C.F.; Lonard, R.I.; Davis, M.R. Using remote sensing and spatial information technologies to detect and map two aquatic macrophytes. *J. Aquat. Plant Manage.* **1999**, *37*, 71–80.
39. Horler, D.N.H.; Dockray, M.; Barber, J. The red edge of plant leaf reflectance. *Int. J. Remote Sens.* **1983**, *4*, 273–288.
40. Curran, P.J.; Dungan, J.L.; Macler, B.A.; Plummer, S.E. The effect of a red leaf pigment on the relationship between red edge and chlorophyll concentration. *Remote Sens. Environ.* **1991**, *35*, 69–76.
41. Filella, I.; Peñuelas, J. The red edge position and shape as indicators of plant chlorophyll content, biomass and hydric status. *Int. J. Remote Sens.* **1994**, *15*, 1459–1470.
42. Gitelson, A.A.; Merzlyak, M.N. Remote estimation of chlorophyll content in higher plant leaves. *Int. J. Remote Sens.* **1997**, *18*, 2691–2697.
43. Knipling, E.B. Physical and physiological basis for the reflectance of visible and near-infrared radiation from vegetation. *Remote Sens. Environ.* **1970**, *1*, 155–159.
44. Elvidge, C.D.; Chen, Z. Comparison of broad-band and narrow red and near-infrared vegetation indices. *Remote Sens. Environ.* **1995**, *54*, 38–48.
45. Cho, H.J.; Kirui, P.; Natarajan, H. Test of multi-spectral vegetation index for floating and canopy-forming submerged vegetation. *Int. J. Environ. Res. Publ. Health* **2008**, *5*, 477–483.

46. Han, L. Spectral Reflectance of *Thalassia Testudinum* with Varying Depths. In Proceedings of 2002 IEEE International Geosciences and Remote Sensing Symposium (IGARSS'02), Toronto, ON, Canada, 24–28 June 2002; pp. 2123–2125.
47. Analytical Spectral Devices Inc. *FieldSpec® UV/VNIR: HandHeld Spectroradiometer User's Guide*; Analytical Spectral Devices Inc.: Boulder, CO, USA, 2002.
48. Poli Control. *Portable Digital/Bench Turbidimeter, Model AP 200 (0–1000 NTU)*; 2012. Available online: www.policontrol.com.br (accessed on 26 October 2012).
49. BioSonics Inc. *DT-X Digital Scientific Portable Echosounder*; 2012. Available online: <http://www.biosonicsinc.com/product-dtx-portable-echosounder.asp> (accessed on 26 October 2012).
50. Sabol, B.M.; Kannenberg, J.; Skogerboe, J.G. Integrating acoustic mapping into operational aquatic plant management a case study in Wisconsin. *J. Aquat. Plant Manage.* **2009**, *47*, 44–52.
51. Johnson, R.A.; Wichern, D.W. *Applied Multivariate Statistical Analysis*, 6th ed.; Pearson Education: Delhi, India, 2007.
52. Clark, R.N.; Roush, T.L. Reflectance spectroscopy: Quantitative analysis techniques for remote sensing applications. *J. Geophys. Res.* **1984**, *89*, 6329–6340.
53. Kruse, F.A.; Lefkoff, A.B.; Boardman, J.W.; Heidebrecht, K.B.; Shapiro, A.T.; Barloon, P.J.; Goetz, A.F.H. The spectral image processing system (SIPS)—Interactive visualization and analysis of imaging spectrometer data. *Remote Sens. Environ.* **1993**, *44*, 145–163.
54. Kruse, F.A.; Lefkoff, A.B.; Dietz, J.B. Expert system-based mineral mapping in northern death valley. California/Nevada. using the Airbone Visible/Infrared Imaging Spectrometer (AVIRIS). *Remote Sens. Environ.* **1993**, *44*, 309–336.
55. Mutanga, O.; Skidmore, A.K.; Kumar, L.; Ferwerda, J. Estimating tropical pasture quality at canopy level using band depth analysis with continuum removal in the visible domain. *Int. J. Remote Sens.* **2005**, *26*, 1093–1108.
56. Youngentob, K.N.; Roberts, D.A.; Held, A.A.; Dennison, P.E.; Jia, X.; Lindernmayer, D.B. Mapping two *Eucalyptus* subgenera using multiple endmember spectral mixture analysis and continuum-removed imaging spectrometry data. *Remote Sens. Environ.* **2011**, *115*, 1115–1128.
57. Ge, S.; Carruthers, R.I.; Krammer, M.; Everitt, H.; Anderson, G.L. Multiple-level defoliation assessment with hyperspectral data: Integration of continuum-removed absorptions and red edges. *Int. J. Remote Sens.* **2011**, *32*, 6407–6422.
58. Carvalho, J.C.; Barbosa, C.C.; Novo, E.M.; Mantovani, J.E.; Melack, J.; Pereira Filho, W. Applications of Quantitative Analysis Techniques to Monitor Water Quality of Curuai Lake, Brazil. In Proceedings of 2003 IEEE International Geosciences and Remote Sensing Symposium, (IGARSS'03), Toulouse, France, 21–25 July 2003; pp. 2362–2364.
59. Krzanowski, W.J.; Marriott, F.H.C. *Multivariate Analysis—Part 2: Classification Covariance Structure and Repeated Measurements*; Arnold: London, UK, 1995.
60. Minitab Inc. *Software Minitab 15*; 2006. Available online: www.minitab.com (accessed on 13 November 2012).
61. Yuhas, R.H.; Goetz, A.F.H.; Boardman, J.W.; Green, R.O. Discrimination among Semi-Arid Landscape Endmembers Using the Spectral Angle Mapper (SAM) Algorithm. In Proceedings of 3rd Annual JPL Airborne Geoscience Workshop, Pasadena, CA, USA, 1–5 June 1992; Volume 1, pp. 147–149.

62. Kruse, F.A.; Boardman, J.W.; Huntington, J.F. Comparison of airborne hyperspectral data and EO-1 Hyperion for mineral mapping. *IEEE Trans. Geosci. Remote Sens.* **2003**, *41*, 1388–1400.
63. Dennison, P.E.; Halligan, K.Q.; Roberts, D.A. A comparison of error metrics and constraints for multiple endmember spectral mixture analysis and spectral angle mapper. *Remote Sens. Environ.* **2004**, *93*, 359–367.
64. Yonezawa, C. Maximum likelihood classification combined with spectral angle mapper algorithm from high resolution satellite imagery. *Int. J. Remote Sens.* **2007**, *28*, 3729–3737.
65. Cho, M.A.; Debba, P.; Mathieu, R.; Naidoo, L.; Aardt, J.V.; Asner, G.P. Improving discrimination of Savanna tree species through a multiple-endmember spectral angle mapper approach: Canopy-level analysis. *IEEE Trans. Geosci. Remote Sens.* **2010**, *48*, 4133–4142.
66. Barbosa, C.C.F. Sensoriamento Remoto da Dinâmica da Circulação da Água no Sistema Planície de Curuai/Rio Amazonas. Ph.D. Thesis, Instituto Nacional de Pesquisas Espaciais, São José dos Campos, Brazil, 2005; p. 281.
67. MathWorks®. *Software MATLAB 7. MATLAB®—The Language of Technical Computing*; 2004. Available online: www.mathworks.com (accessed on 13 November 2012).
68. Han, L. Spectral reflectance with varying suspended sediment concentrations in clear and algae-laden waters. *Photogramm. Eng. Remote Sensing* **1997**, *63*, 701–705.
69. Jensen, J.R. *Remote Sensing of the Environment: An Earth Resource Perspective*, 2nd ed.; Pearson Prentice Hall: Upper Saddle River, NJ, USA, 2007.

© 2013 by the authors; licensee MDPI, Basel, Switzerland. This article is an open access article distributed under the terms and conditions of the Creative Commons Attribution license (<http://creativecommons.org/licenses/by/3.0/>).